Hadron production in $\gamma\gamma$ collisions as a background for e^+e^- linear colliders

Pisin Chen, Timothy L. Barklow, and Michael E. Peskin
Stanford Linear Accelerator Center, Stanford University, Stanford, California 94309
(Received 26 April 1993)

Drees and Godbole have proposed that, at the iteraction point of an e^+e^- linear collider, one expects a high rate of hadron production by $\gamma\gamma$ collisions, providing an additional background to studies in e^+e^- annihilation. Using a simplified model of the $\gamma\gamma$ cross section with soft and jetlike components, we estimate the expected rate of these hadronic events for a variety of realistic machine designs.

PACS number(s): 13.65.+i, 12.38.Bx, 13.87.Ce, 41.60.Ap

I. INTRODUCTION

One of the most important issues in the design of future e^+e^- colliders is the effect of the beam-beam interaction on the physics environment. A linear collider operating at a center-of-mass energy of 400 GeV and above requires a luminosity in excess of $10^{33}\ \mathrm{cm}^{-2}\,\mathrm{sec}^{-1}$. Such a high luminosity can only be achieved by colliding tiny, intense bunches of electrons and positrons. In this circumstance, these bunches interact strongly with one another, producing large numbers of photons and electron-positron pairs [1,2]. This effect potentially creates troublesome backgrounds for experiments on e^+e^- annihilation and must be controlled by adjustment of the collider parameters or the interaction region geometry.

In a recent set of papers, Drees and Godbole [3,4] called attention to another potentially serious background due to the beam-beam interaction, in which photons created by the bunch collision interact to produce hadronic jets. In some designs, the rate of this process exceeds one jet pair per bunch crossing. Under these conditions, each e^+e^- annihilation event would be superposed on an extraneous system of hadronic jets. Thus it is important to evaluate this background systematically and determine its dependence on machine parameters.

In this paper, we will evaluate the rate of hadron and jet production for a variety of accelerator designs which have been proposed for 500-GeV and 1-TeV e^+e^- linear colliders. Three ingredients are needed for such a calculation. The first is the photon-photon luminosity spectrum for the given linear collider design. The second is the cross section for hadron production in photon-photon collisions. The final ingredient is a realistic detector simulation to evaluate what fraction of the produced hadrons is actually seen by the experiments. For the first two of these ingredients, we will present an explicit model which can easily be applied to other accelerator parameters sets. For the third, we will present some illustrative Monte Carlo calculations. We hope that our analysis will make it straightforward to incorporate the constraints of the Drees-Godbole background process in any future proposal for a linear collider. We will also demonstrate that, with an appropriate collider design, the Drees-Godbole background can be reduced to a level where it is quite unimportant.

In Sec. II, we begin our study by reviewing the photon-photon luminosity spectrum at linear colliders. This spectrum is by now well understood. It is given by a sum of contributions from photons radiated from electrons in the scattering process (*bremsstrahlung* photons) and photons created upstream of the photon-photon collision by the coherent action of the electric field of one bunch on the particles of the other (*beamstrahlung* photons). The bremsstrahlung contribution depends almost entirely on the luminosity for e^+e^- collisions. The beamstrahlung contribution depends on the accelerator parameters in a manner which is complicated, but which has by now been worked out in some detail. We will present an explicit parametrization of the photon-photon luminosity spectrum which incorporates these two sources in a convenient form. We will also review the case of a dedicated photon-photon collider, which may be constructed by backscattering laser beams from the electron bunches of an electron linear collider [5–8].

The second ingredient, the value of the photon-photon hadronic cross section, is subject to considerably more uncertainty. One possible model is a vector meson dominance picture in which the photon-photon cross section is taken to be proportional to the ρ-ρ cross section. In their original work, Drees and Godbole [3] took a very different picture, in which the photon-photon cross section originated from the scattering of partons which are constituents of the two photons. This model leads to a cross section which is small at low energies and increases rapidly with energy above the center-of-mass energy of 100 GeV. Both of these features, we believe, are unphysical. Their use of this model has led to considerable confusion, especially in the accelerator physics community, as to the proper way to estimate the important new background source to which they have called attention. In Sec. III, we will attempt to clarify this issue and present a physically reasonable scheme for estimating the photon-photon hadronic cross sections. As Drees and Godbole have stressed, two separate questions must be addressed. First, what is the total cross section for hadron production? Second, what is the rate for hadron production accompanied by QCD jets of 5–20 GeV transverse momentum? Both cross sections can potentially be large enough to lead to rates of order of one event per bunch crossing.

In Sec. III, we will argue that the total cross section is best estimated using vector dominance ideas. This conclusion is in accord with recent high-energy measurements of the of γp total cross section at the DESY ep collider HERA [9,10]. To estimate the cross section for events with jets, we must also invoke the parton-parton cross section for hard scattering. We will evaluate this partial cross section by introducing a very simple model, which we call the reference model. We will explain why we consider the reference model a better description of the structure of jet production than the model of Drees and Godbole. This model follows the essential physics of the "eikonalization" scheme of Forshaw and Storrow [11]. We have modified their model so that it contains no free parameters and is straightforward to apply.

In Sec. IV, we will combine these models of photon spectra and the jet cross section to estimate the rates of hadron and jet production by photon-photon reactions for a wide variety of proposed machines. These calculations depend on the parameters of the machine in a quite straightforward way. We hope that the calculations of this section will be both sufficiently simple and sufficiently informative that they can aid in the estimation of hadronic backgrounds for future stages in the design of e^+e^- linear colliders.

However, as we have already noted, the full effect of hadronic backgrounds cannot be understood without a generating hadronic events and passing them through a realistic detector simulation. The detectors planned for future linear colliders typically have holes in the forward and backward directions and substantial masking to avoid the e^+e^- pairs produced by the beam-beam interaction. Explicit studies of the Drees-Godbole background have shown that much of the hadron production either is lost through these holes or appears at very low energy [12,13]. In Sec. V, we will report a set of Monte Carlo simulations based on the model of hadron production presented in Secs. II and III of this paper. We will quantify the hadronic backgrounds actually detected for some illustrative machine designs, and we will show that these backgrounds are indeed minor effects.

As we were completing this paper, we received two new contributions on the estimation of $\gamma\gamma$ backgrounds in linear colliders [14,15].

II. PHOTON SPECTRA FROM BREMSSTRAHLUNG, BEAMSTRAHLUNG, AND COMPTON BACKSCATTERING

We will describe the spectra which enter $\gamma\gamma$ cross sections at e^+e^- linear colliders in terms of a photon-photon luminosity function $L_{\gamma\gamma}(x_1,x_2)$. Its parameters x_1,x_2 are the fractions of the total energy of the initial electrons and positrons, respectively, carried by the colliding photons. The luminosity function contributes to cross sections as follows:

$$\sigma(e^-(p_1)e^+(p_2)\to X+\text{ anything}) = \int_0^1 dx_1 \int_0^1 dx_2 L_{\gamma\gamma}(x_1,x_2)\sigma[\gamma(x_1p_1)\gamma(x_2p_2)\to X] \ . \tag{2.1}$$

As noted in the Introduction, the luminosity function receives contributions from two sources, beamstrahlung and bremsstrahlung, corresponding to real and virtual photons. Assuming that the sources of the two photons are independent of one another, we can write the luminosity functions for an e^+e^- collider as a sum of components:

$$L_{\gamma\gamma}(x_1,x_2)=f_v(x_1)f_v(x_2) +[f_v(x_1)f_r(x_2)+f_r(x_1)f_v(x_2)] +f_r(x_1)f_r(x_2) \ . \tag{2.2}$$

In this equation, $f_v(x)$ is a modification of the Weizsäcker-Williams distribution for radiation in a collision process and $f_r(x)$ is the average of the beamstrahlung spectrum over the process of interpenetration of the e^- and e^+ bunches. In the cross term, there may be a geometrical suppression of the virtual photon distribution. This effect is important in e^+e^- pair creation at the interaction point in linear colliders [16]. However, the same logic predicts that this effect is negligible for the process considered here.

To compute the jet production cross section at a jet transverse momentum of order Q, Drees and Godbole have argued that one should use a modified version of the standard Weizsäcker-Williams formula. The standard formula integrates over all photon transverse momenta. However, only those photons which are off shell by less than Q^2 can produce jets with transverse momentum of order Q with an unsuppressed rate. In addition, only a fraction c_v of the partons in these photons will be off shell by an amount less than Q^2. By integrating the formula for the equivalent photon distribution given by Brodsky, Kinoshita, and Terazawa [17] up to Q^2 and applying the additional suppression factor, we obtain

$$f_v(x,Q,E)=c_v\frac{\alpha}{2\pi x}\left[[1+(1-x)^2]\left[\ln\frac{Q^2}{m_e^2}-1\right] +\frac{x^2}{2}\left[\ln\frac{1-x}{x^2}+2\right] +\frac{(2-x)^2}{2}\ln\frac{1-x}{(Q^2/E^2+x^2)}\right] , \tag{2.3}$$

where E is the electron beam energy. We will take

$$c_v=0.85 \ , \tag{2.4}$$

following the estimate of Drees and Godbole [3,18]. The distribution (2.3) modifies a simple dependence proportional to $\ln Q^2$ to include the correct enhancement at small x and suppression at large x from the electron kinematics.

In contrast to bremsstrahlung, beamstrahlung occurs in the situation where the scattering amplitudes between the radiating particle and the target particles within the characteristic length add coherently. Typically, for the beam-beam collision in linear colliders there can be over 10^6 target particles involved within the coherence length.

The process can therefore be well described in a semiclassical calculation where the target particles are replaced by their collective electromagnetic (EM) fields.

High-energy e^+e^- beams generally follow Gaussian distributions in the three spatial dimensions, and their local field strength varies inside the beam volume. In the weak disruption limit, where particle motions have small deviations from the z direction, it is possible to integrate the radiation process over this volume and derive relations which depend only on averaged, global beam parameters. The overall beamstrahlung intensity is controlled by a global *beamstrahlung parameter* [19,20]:

$$\Upsilon_0=\gamma\frac{\langle B\rangle}{B_c}=\frac{5}{6}\frac{r_e^2\gamma N}{\alpha\sigma_z(\sigma_x+\sigma_y)}\ , \tag{2.5}$$

where $\langle B\rangle$ is the mean electromagnetic field strength of the beam, $B_c=m_e^2/e\simeq 4.4\times 10^{13}$ G is the Schwinger critical field, N is the total number of particles in a bunch, $\sigma_x,\sigma_y,\sigma_z$ are the nominal sizes of the Gaussian beam, γ is the Lorentz factor of the beam, r_e is the classical electron radius, and α is the fine structure constant. The collective fields in the beam also deform the other beam during collision, by an amount controlled by global *disruption parameters*, which may be different in the two transverse directions [21,22]:

$$D_{x,y}=\frac{2Nr_e\sigma_z}{\gamma\sigma_{x,y}(\sigma_x+\sigma_y)}\ . \tag{2.6}$$

In the most general designs for linear colliders, the photon spectrum due to beamstrahlung is not a factorized function of the electron and positron sources and depends on the detailed evolution of the bunches in the collision process. In general, then, the spectrum of radiation must be computed by detailed simulation [23,19]. However, typical beams in linear colliders are very long and narrow. Since all particles oscillate within the focusing potential that is defined by the geometry of the oncoming beam, the oscillation amplitudes are small compared with their periodicity in z. Then the assumption of small deviations from the z direction remains approximately valid. The main effect of disruption on beamstrahlung is the change of effective EM fields in the bunch due to the deformation of the transverse beam sizes. Thus beamstrahlung is in practice still factorizable even under a non-negligible disruption effect, if one computes its magnitude using an effective beam size which takes the global disruption into account.

The proper value of this effective beam size can be found from the luminosity enhancement factor, defined as the ratio of the effective luminosity to the nominal luminosity due to the change of beam size:

$$H_D\equiv\frac{\bar{\mathcal{L}}}{\mathcal{L}}=\frac{\sigma_x\sigma_y}{\bar{\sigma}_x\bar{\sigma}_y}\ . \tag{2.7}$$

The luminosity enhancement factor is calculable analytically only in the $D\ll 1$ limit. Beyond this limit, the dynamics of the beam-beam interaction becomes nonlinear, and one must use simulations. From the results of these simulations, we can extract scaling laws for H_D and thus for the effective beam size. For the case of round beams ($\sigma_x/\sigma_y=1$), simulations produce the behavior [22]

$$H_D=1+D^{1/4}\left[\frac{D^3}{1+D^3}\right]\{\ln(\sqrt{D}+1)+2\ln(0.8/A)\}\ , \tag{2.8}$$

where $A=\sigma_z/\beta^*$ and β^* is the Courant-Snyder β function at the interaction point. This scaling law is valid to about 10% accuracy. Thus, for round beams, the effective beam size is roughly given by $\bar{\sigma}=\sigma H_D^{-1/2}$.

In realistic designs for high-energy e^+e^- colliders, the beams are intentionally made quite flat, with $R=\sigma_x/\sigma_y$ greater than 5 and as large as 100 in some designs. In this case, there are separate β^* values and separate disruption parameters (2.6) for the x and y directions. Typically, H_{D_x}, computed from (2.8) with $D=D_x$ and $A=\sigma_z/\beta_x^*$, is close to 1, while H_{D_y}, computed from (2.8) using the D_y and σ_z/β_y^*, is large. Since the field strength in a flat charge distribution is mainly determined by σ_x, this means that the disruption effect and its enhancement of beamstrahlung will be relatively mild. However, it turns out that the effect of σ_y is quantitatively important and cannot be neglected.

We therefore suggest the following prescription for computing the effective beamstrahlung parameter: Let [24]

$$\bar{\sigma}_x=\sigma_x H_{D_x}^{-1/2},\quad \bar{\sigma}_y=\sigma_y H_{D_y}^{-1/3}\ . \tag{2.9}$$

The exponent $\frac{1}{3}$ in the second term is determined from computer simulations for very flat beams in which the horizontal particle motion is ignored [22]; a theoretical basis for this scaling law has been proposed in Ref. [25]. Then the effective beamstrahlung parameter is given by

$$\Upsilon=\frac{5}{6}\frac{r_e^2\gamma N}{\alpha\sigma_z(\bar{\sigma}_x+\bar{\sigma}_y)}\ . \tag{2.10}$$

This prescription gives beamstrahlung spectra which agree with the simulation results to an accuracy of 10% for colliders with flat beams ($R>5$).

Once one has an effective value of the beamstrahlung parameter, it is straightforward to derive the photon spectrum [26]. The number of soft photons radiated per unit time, calculated by the classical theory of radiation, is

$$\nu_{\rm cl}=\frac{5}{2\sqrt{3}}\frac{\alpha^2}{r_e\gamma}\Upsilon\ . \tag{2.11}$$

Note that for a given field strength $\nu_{\rm cl}$ is independent of the particle energy. This expression applies to the infrared limit of the spectrum where photon energies approach zero. For a hard photon, up to the initial energy of the electron, the quantum mechanical calculation gives a more general formula:

$$\nu_\gamma=\nu_{\rm cl}[1+\Upsilon^{2/3}]^{-1/2}\ . \tag{2.12}$$

In a multiphoton radiation process, it was found useful to introduce a linear interpolation between these two values.

Let x be the energy fraction of the initial electron carried by the photon. Then define

$$\bar{v}(x)=\frac{1}{1-x}\int_x^1 dx'[x'v_{\rm cl}+(1-x')v_\gamma]$$
$$=\tfrac{1}{2}[(1+x)v_{\rm cl}+(1-x)v_\gamma]\ . \tag{2.13}$$

With these basic parameters introduced, $f_r(x)$ is given by [26]

$$f_r(x)=\frac{1}{\Gamma(\frac{1}{3})}\left[\frac{2}{3\Upsilon}\right]^{1/3}x^{-2/3}(1-x)^{-1/3}$$
$$\times\exp\left[-\frac{2x}{3\Upsilon(1-x)}\right]G(x)\ , \tag{2.14}$$

where Υ is given by (2.10),

$$G(x)=\frac{1-w}{g(x)}\left\{1-\frac{1}{g(x)n_\gamma}[1-e^{-g(x)n_\gamma}]\right\}$$
$$+w\left\{1-\frac{1}{n_\gamma}[1-e^{-n_\gamma}]\right\}\ , \tag{2.15}$$
$$g(x)=1-\frac{\bar{v}}{v_\gamma}(1-x)^{2/3}\ ,$$

and

$$w=\frac{1}{6}\left[\frac{3\Upsilon}{2}\right]^{1/2},\quad n_\gamma=\sqrt{3}\sigma_z v_\gamma\ . \tag{2.16}$$

n_γ is the mean number of photons radiated per electron throughout the collision. The approximations are valid for $\Upsilon\lesssim 5$.

So far, we have been discussing the photon spectra associated with linear colliders operating in a mode to study e^+e^- collisions. It is also possible to run a linear collider in a mode dedicated to the study of $\gamma\gamma$ collisions, by backscattering a laser beam from each electron beam just before the collision point. The luminosity for photon-photon collisions should be essentially equal to the design luminosity for e^+e^- collisions, without the enhancement factor (2.7). Ten years ago, Ginzburg *et al.* [5] studied this possibility in some detail and displayed many interesting characteristics of the photon-photon collider. In particular, they computed the luminosity spectrum of each photon beam. Ignoring polarization effects,

$$f_c(x)=\frac{1}{\mathcal{N}}\left[1-x+\frac{1}{1-x}-\frac{4x}{X(1-x)}+\frac{4x^2}{X^2(1-x)^2}\right], \tag{2.17}$$

where

$$\mathcal{N}=\left[1-\frac{4}{X}-\frac{8}{X^2}\right]\ln(1+X)+\frac{1}{2}+\frac{8}{X}-\frac{1}{2(1+X)^2}\ . \tag{2.18}$$

The parameter X is related to the center-of-mass energy of the electron-laser photon collision, $X=(E_{\rm c.m.}/m_e)^2$, and x is restricted to $x<X/(1+X)$. Telnov [27] has argued that the optimal value of X is $X=2+\sqrt{8}\approx 4.83$, and we will use this value here. The luminosity function for the $\gamma\gamma$ collider is then simply

$$L_{\gamma\gamma}(x_1,x_2)=f_c(x_1)f_c(x_2)\ . \tag{2.19}$$

The formulas tabulated in this section give a complete and rather straightforward method for computing the photon spectrum relevant to background processes at future linear colliders.

III. $\gamma\gamma$ TOTAL CROSS SECTION

In order to compute hadronic backgrounds due to the photon spectrum described in Sec. II, we must fold this spectrum with a reasonable theory of the photon-photon hadronic cross section. Unfortunately, this cross section has been measured only at very low energies—energies below 20 GeV in the center of mass. The extrapolation of these measurements even to 100 GeV in the center of mass depends on the theoretical models. In this section, we will describe a simple, specific model which we propose should be taken as a reference.

The simplest model of the energy dependence of the photon-photon hadronic cross section is that given by vector meson dominance. In this model, the photon is considered to resonate, with some amplitude, to a hadronic state such as the ρ. Then the photon-photon total cross section should be proportional to the ρ-ρ total cross section as a function of energy. In practice, among the hadronic total cross sections, only the pp and $p\bar{p}$ cross sections are measured above 30 GeV in the center of mass. We will estimate the energy dependence of the photon-photon total cross section by averaging these to remove the effects of baryon exchange. Using the parametrization of Amaldi *et al.* [28] [which continues to fit the more recent CERN Super Proton Synchrotron (SPS) and Fermilab data], we have

$$\sigma(\gamma\gamma\to\ \text{hadrons})=\sigma_0\{1+(6.30\times10^{-3})[\ln(s)]^{2.1}$$
$$+(1.96)s^{-0.37}\}\ , \tag{3.1}$$

where s is given in $(\text{GeV})^2$. The same formula, with $\sigma_0=80\ \mu$b, describes the new high-energy determinations of the γp total cross section from HERA [9,10]. To describe $\gamma\gamma$ scattering, the constant may be adjusted so that $\sigma(\gamma\gamma)=[\sigma(\gamma p)]^2/\sigma(pp)$ in the region of approximately constant cross sections at $E_{\rm c.m.}\sim 30$ GeV:

$$\sigma_0=200\ \text{nb}\ . \tag{3.2}$$

The formula (3.1) is plotted in Fig. 1 and compared to direct determinations of the $\gamma\gamma$ hadronic cross section [29–31]. Comparing $\sigma(\gamma p)$ to $\sigma(\pi p)$, we conclude that the photon is a hadron a fraction $\frac{1}{400}$ of the time.

A second model of the photon-photon cross section is one based on parton-parton scattering. Many authors have speculated that the hard QCD processes can make a significant contribution to the total cross section in hadron-hadron scattering at high energies. Drees and Halzen [32] proposed that parton-parton scattering could be the dominant process in the photon-hadron cross sec-

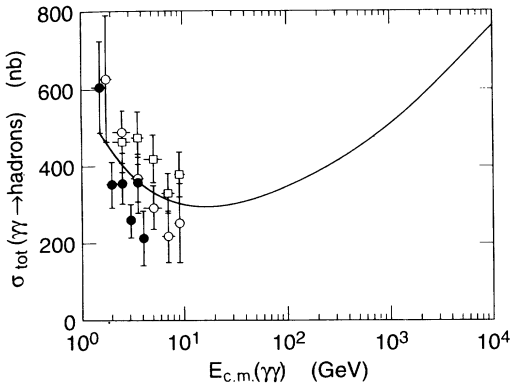

FIG. 1. Parametrization of the photon-photon total hadronic cross section, Eq. (3.1), compared to data from Refs. [29] (circles), [30] (squares), [31] (dots).

tion above 100 GeV in the center of mass and that this mechanism would lead to photon-hadron cross sections which rise much faster than (3.1). This theory of the photon-hadron cross section was then taken over by Drees and Godbole to describe the photon-photon hadronic cross section. However, this theory has been criticized in both contexts by many authors. Let us first write out a simple, quantitative version of the Halzen-Drees-Godbole theory and then explain how this theory should be used in the calculation of hadronic backgrounds.

At the most naive level, the cross section for hadron production by hard parton-parton scattering is given by folding the parton scattering cross sections computed in QCD with the experimentally determined parton distributions. In general, this cross section is infrared divergent and requires a cutoff at low momentum transfer or transverse momentum. Drees and Halzen noted that one can obtain cross sections of the order of the expected total cross section for hadron production if one takes this cutoff to be a few GeV. In this calculation, the most important effect comes from gluon-gluon scattering at small momentum fractions.

Let us define the jet yield $\mathcal{Y}(p_*)$ as the expected number of jets with $p_\perp > p_*$, divided by the luminosity. The simplest hard-scattering theory of the total cross section would be to take

$$\sigma(\gamma\gamma) = \sigma_0 + \tfrac{1}{2}\mathcal{Y}(p_*) , \tag{3.3}$$

where σ_0 is a constant soft-scattering cross section and the cutoff p_* is taken sufficiently large that events contributing to the jet yield are not also accounted as part of σ_0. Let us first describe how we evaluate $\mathcal{Y}(p_*)$ and then discuss its relation to the total cross section.

We compute $\mathcal{Y}(p_*)$ from the formula

$$\mathcal{Y}(p_*) = \int_0^1 dz_1 F(z_1) \int_0^1 dz_2 F(z_2) \int_{-1}^1 d\cos\theta \frac{d\sigma}{d\cos\theta}(gg \to gg)\theta(p_\perp - p_*) . \tag{3.4}$$

In this formula, θ is the center-of-mass parton-parton scattering angle. We take the parton distribution $F(z)$ to be the sum of gluon and quark distributions [33],

$$F(z) = f_g(z) + \tfrac{4}{9}\sum_i [f_{qi}(z) + f_{\bar{q}i}(z)] , \tag{3.5}$$

with the appropriate coefficient that we can approximate all of the parton cross sections by the gluon-gluon cross section:

$$\frac{d\sigma}{d\cos\theta}(gg \to gg) = \frac{9}{16}\frac{\pi\alpha_s^2}{\hat{s}}\left[\frac{(2+\cos^2\theta)^3}{\sin^4\theta}\right] , \tag{3.6}$$

where $\hat{s} = z_1 z_2 s$ is the square of the gluon-gluon center-of-mass energy. The coupling constant α_s is evaluated at the momentum scale $p_\perp$. We compute α_s from leading-order evolution with four flavors and $\Lambda = 400$ MeV [α_s (3 GeV) = 0.37], the convention of Drees and Godbole.

For the parton distributions of the photon, we use the parameterization of Drees and Grassie [34]. The gluon distribution in the photon is poorly known experimentally. However, this distribution should be calculable theoretically to rough accuracy by integrating the Altarelli-Parisi equations, taking as an initial condition at $Q \sim 300$ MeV the parton distributions of a meson, multiplied by the probability (in vector dominance) that the photon resonates with a meson. Although Drees and Grassie took their initial condition from the early photon-photon scattering data from the DESY e^+e^- collider PETRA, their result actually agrees with the result of this more theoretical method. Unfortunately, determinations of the photon structure functions directly from two-photon data [35,36] have a larger spread than the error of about 30% that we assign to this method.

The QCD result for the gluon-gluon scattering cross section at low momentum transfer has much larger uncertainties. First of all, the lowest-order QCD result receives large perturbative corrections. There are further corrections which come from outside the standard leading-logarithmic diagrams of QCD. On the one hand, the summation of diagrams relevant to multiple gluon production reveals that gluon-gluon scattering is controlled by a Regge pole which increases the cross section proportional to a (small) power of the gluon-gluon center-of-mass energy [37]. On the other hand, because the photon is a total color singlet, the amplitudes for creating low-transverse-momentum gluons should exhibit cancellations between the various color sources [38]. Both classes of corrections are beyond the scope of this paper. From here on, we will consider (3.4) as a standard reference point for the calculation of jet production. We expect that it yields a calculation of $\mathcal{Y}(p_*)$ up to an uncertainty of about a factor of 2.

This said, we present in Fig. 2 the result of evaluating $\mathcal{Y}(p_*)$. From the simplest point of view, this is a theory of the photon-photon hadronic cross section: $\sigma \sim \frac{1}{2}\mathcal{Y}(p_*)$, for an appropriately chosen value of p_*.

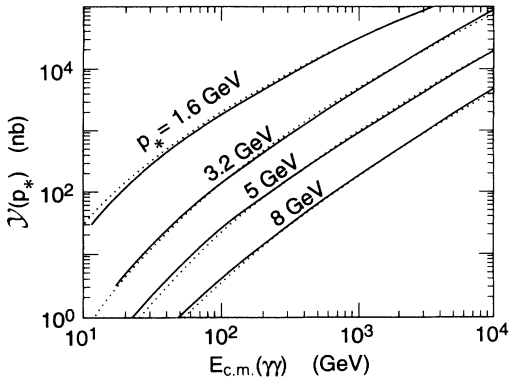

FIG. 2. Jet yields predicted by the formula (3.4), for $p_* = 1.6$, 3.2, 5, and 8 GeV, shown as a function of the $\gamma\gamma$ center-of-mass energy. The dotted curves show the parametrization of this quantity given in (3.7).

This is, in fact, the theory applied by Drees and Godbole, with the parameter choice $p_* = 1.6$ GeV [4]. Note that for any value of p_*, this prediction for the cross section rises much faster at high energy than the expectation from (3.1). In addition, this prediction for the cross section is very small at low energy, since it does not include the effects of soft hadronic reactions. The dependence of the jet yield on energy and p_* is well described by the parameterization

$$\mathcal{Y}(p_*, E_{c.m.}) = A_1 \frac{(E_{c.m.})^{A_2}}{(A_3 + p_*)^2} \times \exp\left\{ -\frac{B_1(p_*)}{(E_{c.m.} - p_*)^{B_2(p_*)}} \right\}, \quad (3.7)$$

where $\mathcal{Y}$ is given in nanobarns, energies are in GeV, $A_1 = 4000$, $A_2 = 0.82$, $A_3 = 3.0$, and

$$B_1(p_*) = 14.2 \tanh(0.43 p_*^{1.1}), \qquad B_2(p_*) = 0.48/p_*^{0.45}. \quad (3.8)$$

This parametrization fits our numerical evaluation to within 20% accuracy for $p_* < 10$ GeV and $E_{c.m.} < 10$ TeV. As we have emphasized, the numerical evaluation itself is considerably more uncertain. We used this parameterization in the computations reported in Sec. IV.

However, it has been argued that the photon cross sections cannot rise as fast as the jet yield is predicted to rise in Fig. 2 [39,40]. The easiest way to argue to this conclusion is to redo the analysis just described for $p\bar{p}$ collisions and compare the results to the data on the $p\bar{p}$ total cross section. This comparison is shown in Fig. 3(a). Note that the jet yield calculation using the Drees-Godbole value of p_* is completely incompatible with the $p\bar{p}$ total cross section in a region where this cross section is well measured. A similar comparison can now be made in photoproduction following the new HERA measurements, and this in shown in Fig. 3(b).

In addition to the total cross section, the UA1 experiment has reported measurements of the cross section for events with jet activity, by counting events with a fixed deposition of transverse energy in a circle of radius 1 in the plane of rapidity and azimuthal angle [42]. In this paper, the experimenters argued that such minijet events are well defined only for values of the transverse energy of a cluster above 5 GeV. In Fig. 3(a), we show their results for the cross section for producing clusters of 5 GeV transverse energy and the comparison of this cross section to half the jet yield for a parton transverse momentum cutoff $p_* = 3.2$ GeV. At the time of these measurements, Pancheri and Srivastava [43] pointed out that this cross section could be fit by a simple QCD estimate with a value of p_* reduced from the observed transverse energy. The comparison shown in Fig. 3 fixes the size of this reduction for the Drees-Godbole conventions. To estimate the cross section for events with clusters of 10 GeV transverse energy, we will use $p_* = 8$ GeV.

The idea that minijets with only 5 GeV of transverse energy are produced independently of the underlying minimum-bias multiple-particle production is still controversial. It is possible that a model with incoherently produced jets makes sense at values of the transverse energy of 10 GeV or above. When we evaluate jet cross sections later is this paper, we will also illustrate the dependence of our results on the transverse momentum cutoff p_*.

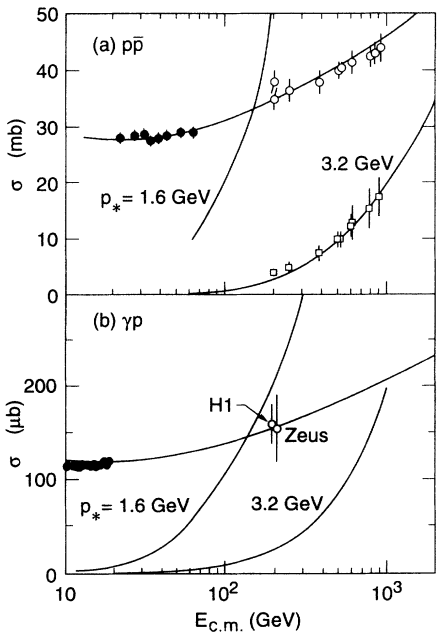

FIG. 3. (a) Comparison of the jet yield in $p\bar{p}$ collisions to the observed total cross section. The data are taken from Ref. [42]. The upper set of data points represents measurements of the inelastic $p\bar{p}$ cross section; these measurements are well fit by the formula of Ref. [28]. The lower set of data points represents the UA1 measurements of the jet cross section as described in the text. The two curves show the energy dependence of $\frac{1}{2}\mathcal{Y}(p_*)$ for $p\bar{p}$ collisions, for $p_* = 1.6$ and 3.2 GeV. (b) Comparison of the jet yield in γp collisions to the observed total cross section. The data is taken from Refs. [41,9,10]. The smooth curve through these points is proportional to (3.1). The two rising curves show the energy dependence of $\frac{1}{2}\mathcal{Y}(p_*)$ for γp collisions, for $p_* = 1.6$ and 3.2 GeV.

We will now argue that, in photon-photon collisions, we should see the same disagreement between the actual total cross section and the jet yield calculation at high energy. At low energies, photon-photon collisions have an approximately constant hadronic cross section from vector dominance: Each photon resonates, with a certain probability, to a hadron, and these hadrons collide with a certain total cross section. Taking the probability that the photon is a hadron to be the value $\frac{1}{400}$ given above and taking the maximum hadronic cross section to be that of a disk of radius 1 fm, we obtain an estimate

$$\sigma_T(\gamma\gamma \to \text{hadrons}) \sim 300 \text{ nb} , \tag{3.9}$$

which is in reasonable agreement with (3.1). In order to produce a significantly larger cross section, either the photon must become larger or it must become a hadron with higher probability. Resolving the hadronic components of the photon into partons does not increase the size of the photon. Altarelli-Parisi evolution can create new hadronic components of the photon, through the diagram in which the photon, off shell by an amount Q, splits to a $q\bar{q}$ pair. This diagram has a substantial effect on the total number of gluons in the photon, but it has only a small effect on the photon's hadronic cross section, since the new hadronic component has the very small size π/Q^2. It is possible to explain a slowly rising cross section by making a model in which the soft hadron is a grey scattering distribution which becomes black as the gluon-gluon scattering becomes important. As the disk becomes black, the effect of gluon-gluon scattering on the total cross section must turn off. This physical effect can be implemented in a calculational scheme called "eikonalization." For the case of γp scattering, explicit models of this sort have been constructed by Forshaw and Storrow [44] and Fletcher, Gaisser, and Halzen [45]. Forshaw and Storrow have also written an eikonalized model of the $\gamma\gamma$ cross section [11]. Qualitatively, these eikonalized models have a slowly rising total cross section similar to that of (3.1). An example of such a model which fits the rise of the pp cross section has been given in Ref. [46]. On the other hand, it is possible that parton hard scattering has nothing to do with the observed rise in the pp cross section at high energy. In this paper, we will adopt the most straightforward course, that of taking the formula (3.1) literally as a first approximation to the energy dependence of the cross section for hadron production in $\gamma\gamma$ collisions.

However, we are also interested to know the cross section for hadronic reactions which contain hard QCD jets. It is quite possible that ordinary, low-$p_\perp$ hadronic events produce little complication when superposed on high-energy e^+e^- annihilation events, but that hadronic events with jets produce troublesome complications. Thus we need to estimate backgrounds from events with jet production. We emphasize that we are concentrating on the case of jets with transverse momentum below 20 GeV which appear as the result of a second collision at the same beam crossing as the e^+e^- annihilation. Above this transverse momentum, parton-parton scattering decreases in importances as a source of hadronic jets relative to quark-photon and direct photon-photon scattering processes (the processes Drees and Godbole call "once-resolved" and "direct") [3]. However, these latter events are too rare to appear superposed on a significant number of e^+e^- annihilation events.

To a first approximation, the jet yield $\mathcal{Y}(p_*)$ computed from (3.4) should be a valid estimate of the total number of jets produced even when the jet yield substantially overestimates the total hadronic cross section. The reason for this is that the individual parton-parton interactions are relatively weak, and it is only because there are many gluons in a hadron that the sum of these cross sections saturates the geometrical limit on the cross section. In other words, those events in which the hadronic disks overlap typically contain a soft interaction plus gluon-gluon scatterings; if $\mathcal{Y}(p_*) \gg \sigma$, typical encounters contain many individual gluon-gluon collisions. If we assume that these collisions are completely independent, we would expect the number of pairs of jets per event to follow a Poisson distribution, such that the mean number of jets per event is

$$\langle n_{\text{jet}} \rangle = \mathcal{Y}(p_*)/\sigma . \tag{3.10}$$

The cross section for events with jets of $p_\perp > p_*$, in this model, is

$$\sigma(p_*) = \sigma\{1 - \exp[-\mathcal{Y}(p_*)/2\sigma]\} . \tag{3.11}$$

If the mechanism of scattering changes as a function of the impact parameter, as is true in eikonal models, there will be small corrections to this simple model. We will ignore them.

The combination of these ideas has an interesting implication. $\mathcal{Y}(p)$ increases much more rapidly with energy than σ. However, in this picture, the main effect of the increase in $\mathcal{Y}(p_*)$ is not to increase the hadronic cross section, but rather to increase the number of jets per event. For photon-photon collisions and for hadron-hadron collisions, above 1 TeV in the center of mass, we expect that the typical event is bristling with jets of 10 GeV transverse momentum. In Fig. 4, we illustrate the time structure of events at an e^+e^- collider in a naive model and in what we feel is a more correct model of jet production. The latter case casts the problem of hadronic jets underlying e^+e^- annihilation events in a quite

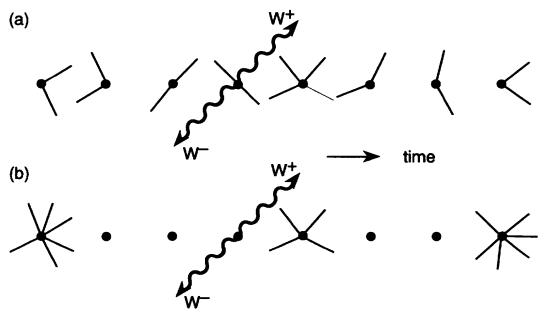

FIG. 4. Time structure of e^+e^- reactions in a linear collider. The dots represent individual bunch crossings. In the naive model (a), the minijet are distributed evenly among bunch crossings. The model (b) has a much smaller $\gamma\gamma$ hadronic cross sections, but the same large value of the jet yield.

different form and one which is probably much easier to ameliorate. In Fig. 5, we show the energy dependence of the mean number of jets in $\gamma\gamma$ collisions with hadron production, according to our model, for various values of the transverse momentum. In Fig. 6, we show the corresponding predictions for the total cross section for a $\gamma\gamma$ collision to produce events with parton scattering at these values of transverse momentum. We have already noted that the results for the lowest value of p_* are probably academic, since such small minijets cannot be distinguished in hadron-hadron collisions. The two curves with $p_*=3.2$ and 8 GeV correspond to events with clusters of 5 and 10 GeV transverse energy.

Since Fig. 5 predicts a relatively large number of jets per hadronic event, one might hope that multiple jet events could be recognized experimentally in γp or $p\bar{p}$ collisions at accessible energies. Unfortunately, our model gives fewer jetlike events in these processes, since the gluon distribution in the proton is softer than that in the photon. For $p_*=3.2$ GeV, we estimate an average of 0.15 jet pairs for γp collisions at 200 GeV and an average of 0.6 jet pairs for $p\bar{p}$ collisions at 2 TeV. However, we expect two jet pairs per minimum-bias event at the Superconducting Super Collider (SSC) energy of 40 TeV, so that the phenomenon of multiple minijets may become observable at the SSC.

In our model, jet cross sections eventually saturate at the value of the total cross section. Thus we must give some thought to the value of Q we should use in computing $\gamma\gamma$ total cross sections from the virtual photon distribution function (2.3). The logarithm in (2.3) comes from an integral over photon transverse momentum. Ordinarily, to evaluate total cross sections due to soft processes, one would cut off this integral at a momentum characteristic of the soft momentum transfer, of order 1 GeV. To compute the cross section for a hard process, one would run this integral up to the momentum transfer of the hard process and, therefore, take $Q=p_*$. However, when the cross section for a hard process with momentum transfer P is comparable to the total cross section, photons with transverse momenta up to this value contribute strongly to the total cross section, and we must

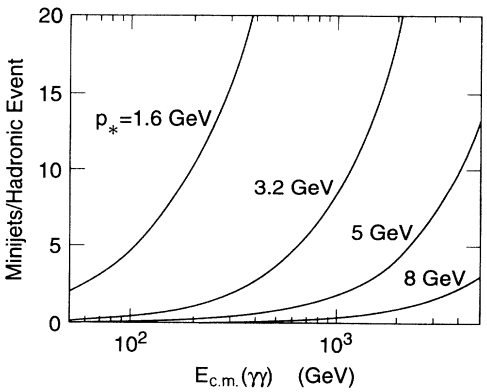

FIG. 5. Number of jets with transverse momentum greater than p_* per hadronic $\gamma\gamma$ event, for $p_*=1.6$, 3.2, 5, and 8 GeV, according to the model of Eq. (3.10). The ordinate is the $\gamma\gamma$ center-of-mass energy.

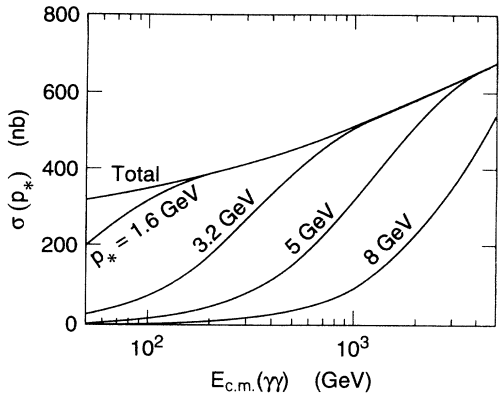

FIG. 6. Cross sections for hadron production in $\gamma\gamma$ collisions accompanied by jets of transverse momentum greater than p_*, for $p_*=1.6$, 3.2, 5, and 8 GeV, according to the model of Eq. (3.11). The ordinate is the $\gamma\gamma$ center-of-mass energy.

take $Q\sim P$ also to compute the total cross section. Using (3.7), we estimated this value as a function of energy. Thus, in evaluating virtual photon cross sections for jets with transverse momentum p_*, we choose Q in $f_v(x,Q)$ according to the prescription

$$Q=\max[p_*,Q_H(E),1\text{ GeV}]\ , \tag{3.12}$$

where $Q_H=(E/10.0)^{0.43}$ and E is the $\gamma\gamma$ center-of-mass energy in the collision.

We will refer to the model for the $\gamma\gamma$ hadronic cross section given in (3.1), (3.4) or (3.7), (3.10), and (3.11) as the reference model (RM). We feel that this model is the best compromise available between simplicity and plausibility in the theoretical extrapolation of the $\gamma\gamma$ hadronic cross section. We emphasize that the results of this model related to jet production are expected to be uncertain to at least a factor of 2.

At some points in the following section, we will compare the predictions of this model to two additional models which represent the extreme behaviors possible for this hadronic cross section. On the one hand, there is the constant cross section (CC) model, in which we take

$$\sigma(\gamma\gamma\to\text{hadrons})=300\text{ nb}\ , \tag{3.13}$$

independent of energy. On the other hand, there is a model which we will call the minijet dominance (MD) model:

$$\sigma(\gamma\gamma\to\text{ hadrons})=300\text{ nb}+\tfrac{1}{2}\mathcal{Y}(p_*)\ , \tag{3.14}$$

with the choice $p_*=1.6$ GeV. This is not exactly the model advocated by Drees and Godbole; they omit the constant term, and at the end of Ref. [4], they argue that the jet yield estimate should be modified in a manner similar to what we have described above. However, this model captures the spirit of the explicit calculations that they have performed, in a way that can be easily compared with our reference point.

IV. HADRON PRODUCTION RATES

Having now specified our model completely, we can make use of it to predict the rate of hadronic $\gamma\gamma$ events

to be expected at future colliders. In this section, we will present the results of applying this model to a variety of specific collider designs, for center-of-mass energies of 500 GeV and 1 TeV, both for e^+e^- and for $\gamma\gamma$ collisions. Our set of sample collider parameters is given in Tables I and II. Table I gives a set of designs for 0.5-TeV colliders presented at the 1992 Linear Collider Conference [47]. Table II gives a set of designs corresponding to extensions of the 0.5-TeV machines to 1.0 TeV in the center of mass [48].

Before beginning the analysis of specific designs, we would like to present some results which appear as general scaling laws, independent of the details of the collider. This will also give us an opportunity to compare our reference model (RM) with the minijet dominance (MD) model and constant cross section (CC) model defined at the end of the previous section.

In a linear e^+e^- collider, the rate of hadronic $\gamma\gamma$ events per bunch crossing is obtained as a convolution of the photon spectra from bremsstrahlung and beamstrahlung. If we ignore beamstrahlung and consider the rate from bremsstrahlung alone, our results will be independent of the detailed collider design and, for a fixed design energy, will simply be proportional to the luminosity per electron-positron bunch crossing. This is also true for the full rate of hadronic events in the case where the machine is converted to a $\gamma\gamma$ collider by backscattering laser beams, since, in that case, the energy distribution of backscattered photons is fixed by the physics of Compton scattering. As a reference point close to most current designs, we will assume a design luminosity of

$$\mathcal{L}=10^{34}\left[\frac{E_{\text{c.m.}}}{1\ \text{TeV}}\right]^2 \text{cm}^{-2}\,\text{sec}^{-1}\,. \tag{4.1}$$

In typical designs, this luminosity is divided into pulses which are produced at a repetition rate of roughly $f_{\text{rep}}\sim 100/\text{sec}$. In the most recent designs, which have been inspired by attempts both to raise the design luminosity and to reduce the Drees-Godbole background, the electron and positron pulses are divided into trains of order $n_b\sim 100$ bunches, which we will assume can be distinguished in time by the detector. Thus we take as our reference value a luminosity per bunch crossing equal to 10^{-4} sec times (4.1), that is,

$$\mathcal{L}_1=\mathcal{L}/(f_{\text{rep}}n_b)=10^{-3}\left[\frac{E_{\text{c.m.}}}{1\ \text{TeV}}\right]^2 \text{nb}^{-1}\,. \tag{4.2}$$

For any specific machine, the results for bremsstrahlung- or laser-photon-induced hadronic backgrounds can be obtained by scaling the luminosity per bunch crossing up or down from this value.

The assumption that the hadrons produced at each bunch crossing can be distinguished in time is crucial to our analysis and deserves some further comment. This assumption is more or less restrictive depending on which of the specific collider designs in the tables is being considered. In designs such as TeV Electron Superconducting Linear Accelerator (TESLA), based on superconducting rf cavities, the bunch spacing is typically of order 1 μsec, and there is no problem timing tracks to much higher accuracy. However, in the designs based on con-

TABLE I. Parameters and hadronic backgrounds for 0.5-TeV linear colliders.

Linear colliders	CLIC	DLC	JLC	NLC	TESLA	VLEPP
$\mathcal{L}$ ($10^{33}\text{cm}^{-2}\,\text{sec}^{-1}$)	2.7	2.4	6.8	6.0	2.6	12
f_{rep} (Hz)	1700	50	150	180	10	300
n_b	4	172	90	90	800	1
$\mathcal{L}_1$ (10^{-3} nb^{-1})	0.40	0.27	0.50	0.37	0.33	40
N (10^{10})	0.6	2.1	0.7	0.65	5.15	20
σ_x/σ_y (nm)	90/8	400/32	260/3	300/3	640/100	2000/4
σ_z (μm)	170	500	80	100	1000	750
β_x^*/β_y^* (mm)	2.2/0.16	16/1	10/0.1	10/0.1	10/5	100/0.1
D_x/D_y	1.3/15	0.70/8.8	0.09/8.2	0.08/8.2	1.25/8.0	0.43/—
A_x/A_y	0.08/1.06	0.03/0.5	0.008/0.8	0.01/1.0	0.1/0.2	0.008/—
$\bar{\sigma}_x/\bar{\sigma}_y$ (nm)	40/5.5	246/19	259/2.0	300/2.2	304/50	1587/4
H_D	3.3	2.8	1.5	1.4	4.2	1.3
$\bar{\mathcal{L}}$ (10^{33} cm$^{-2}\,\text{sec}^{-1}$)	8.80	6.67	10.1	8.22	11.1	15.1
$\bar{\mathcal{L}}_1$ (10^{-3} nb^{-1})	1.30	0.76	0.74	0.51	1.39	50.2
Υ_0	0.16	0.043	0.15	0.095	0.031	0.059
Υ	0.35	0.071	0.15	0.096	0.065	0.074
δ_B	0.36	0.08	0.05	0.03	0.14	0.14
n_γ	4.6	3.1	1.0	0.84	5.8	5.1
e^+e^- mode						
N_{had}	1.37	0.32	0.07	0.04	1.57	45.3
N_{jet} (10^{-2})	5.80	0.44	0.22	0.10	1.62	56.2
N_{jet10} (10^{-4})	16.4	1.16	0.69	0.31	3.90	139
$\gamma\gamma$ mode						
N_{had}	0.15	0.10	0.19	0.14	0.13	15.2
N_{jet5} (10^{-2})	6.90	4.72	8.61	6.43	5.68	685
N_{jet10} (10^{-4})	32.4	22.3	40.7	30.4	26.9	3240

TABLE II. Parameters and hadronic backgrounds for 1.0-TeV linear colliders.

Linear colliders	DLC	JLC	NLC	TESLA
$\mathcal{L}$ (10^{33} cm^{-2}sec^{-1})	2.5	8.8	12.8	10.6
$f_{\rm rep}$ (Hz)	50	150	90	10
n_b	50	20	90	800
$\mathcal{L}_1$ (10^{-3} nb^{-1})	0.99	2.17	1.58	1.31
N (10^{10})	2.8	1.8	1.3	5.8
σ_x/σ_y (nm)	223/28.3	372/3.2	425/2	404/50.5
σ_z (μm)	500	113	100	1100
β_x^*/β_y^* (mm)	5/0.8	24.6/0.12	40/0.1	8/2.5
D_x/D_y	1.40/11.0	0.08/9.7	0.04/8.5	1.95/15.6
A_x/A_y	0.1/0.625	0.005/0.9	0.0025/1.0	0.14/0.44
$\bar{\sigma}_x/\bar{\sigma}_y$ (nm)	100/17.1	372/2.2	425/1.5	172/27.0
H_D	3.7	1.5	1.4	4.4
$\bar{\mathcal{L}}$ (10^{33} cm^{-2}sec^{-1})	9.2	12.8	17.5	46.6
$\bar{\mathcal{L}}_1$ (10^{-3} nb^{-1})	3.70	3.10	2.18	5.86
Υ_0	0.20	0.38	0.27	0.10
Υ	0.42	0.38	0.27	0.24
δ_B	0.53	0.14	0.07	0.50
n_γ	8.1	1.7	1.1	10.4
e^+e^- mode				
$N_{\rm had}$	15.3	0.83	0.34	40.1
$N_{\rm jet5}$	1.53	0.09	0.03	2.65
$N_{\rm jet10}$ (10^{-2})	5.53	0.37	0.12	8.54
$\gamma\gamma$ mode				
$N_{\rm had}$	0.42	0.93	0.68	0.56
$N_{\rm jet5}$	0.31	0.68	0.50	0.41
$N_{\rm jet10}$ (10^{-2})	2.50	5.61	4.10	3.40

ventional cavities, the length of a bunch train cannot be greater than a few hundred nsec, and so the spacing of bunches must be proportionately smaller. In the Next Linear Collider (NLC) design, for example, the bunch spacing is only 1.4 nsec. However, we do not feel that this is unreasonably small. The drift chamber of the Mark II experiment at the SLAC Linear Collider (SLC) could time tracks to a resolution of 1 nsec, even though it was not optimized for this feature. Energy clusters in a calorimeter can be given time stamps with 1 nsec resolution or better by adding layers of timing detectors, such as scintillation counters, to the calorimeter. The time between bunch train crossings is quite long (5.6 and 11.1 msec for the 500- and 1000-GeV NLC designs, respectively) so that one can make use of timing detectors with large recovery times.

Now we present our estimates of $\gamma\gamma$ background rates for the reference machine defined above, as a function of its energy. We consider first e^+e^- colliders, ignoring beamstrahlung. In Fig. 7(a), we plot the total rate of $\gamma\gamma$ background events, as a function of the design energy of the machine, assuming the specific luminosity (4.2). The $\gamma\gamma$ cross section is integrated over all solid angles and down to a $\gamma\gamma$ center-of-mass energy $E_{\gamma\gamma}$ of 5 GeV. Note that the MD model predicts a much higher level of background, while the RM and CC models are actually quite close in their predictions. Under the assumptions of the RM model and assuming that the multibunch operation called for in (4.2) is indeed feasible, the total rates of hadronic background seem to be tolerable without a need for further analysis for e^+e^- colliders of energy up to 2

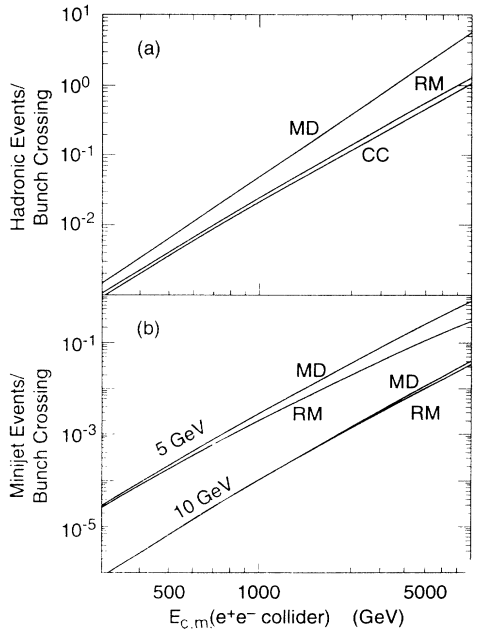

FIG. 7. Comparison of the predictions of three models of the $\gamma\gamma$ total cross section for the rate of hadronic background events in e^+e^- colliders. Beamstrahlung is ignored, and the luminosity per bunch crossing is taken to have the canonical dependence (4.2): (a) predictions of the RM, MD, and CC models (described in the text) for the total rate of $\gamma\gamma$ events; (b) predictions of the RM and MD models for the rate of events with observable minijets of transverse energy 5 and 10 GeV.

TeV. Unfortunately, the assumption of ignoring beamstrahlung breaks down well before this point.

In Fig. 7(b), we show the corresponding predictions for hadronic events with observable QCD jets, using the MD and RM models with transverse energies above 5 GeV (computed at $p_* = 3.2$ GeV) and 10 GeV (computed at $p_* = 8$ GeV). Again, we integrate over $E_{\gamma\gamma} > 5$ GeV. As the jet transverse momentum increases, the MD and RM models come into closer agreement. In addition, the number of events is substantially smaller, especially at e^+e^- energies of 1 TeV and below.

At this point in the analysis, it is not clear whether the true figure of merit for assessing the hadronic background at linear colliders is given by the total rate of hadronic events or only the rate for events containing jets. In Sec. V, we will report simulation results which indicate that both rates play a role in determining the hadronic backgrounds. Events with jets are more effective in depositing unwanted background energy, but events of the minimum-bias type can also have some effect. As we proceed to discuss specific collider designs, we will present the total rate of hadronic events and also the rate of jet events for $p_* = 3.2$ and 8 GeV. Taking these three numbers together, one can obtain a feel for the general character of the hadronic background.

In Figs. 8(a) and 8(b), we show the results of calculations similar to those of the previous figure for $\gamma\gamma$ colliders. Again, we assume the luminosity per bunch (4.2); essentially, we are assuming that high-energy electrons can be converted, one to one, to photons. As Drees and Godbole pointed out, the results for this case are about an order of magnitude higher than the bremsstrahlung contribution for 500-GeV machines, rise faster with energy, and are considerably more model dependent. It is comforting, at least, that, according to our reference model, a 500-GeV $\gamma\gamma$ collider based on most current e^+e^- collider designs should not have a serious problem with its $\gamma\gamma$ background.

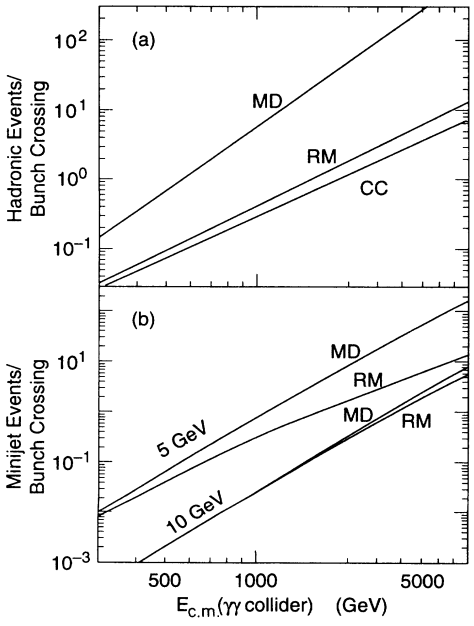

FIG. 8. Comparison of the predictions of three models of the $\gamma\gamma$ total cross section for the rate of hadronic background events in $\gamma\gamma$ colliders. The conventions are as in Fig. 7.

It is interesting not only to know the total number of $\gamma\gamma$ hadronic events, but also their distributions in the various kinematic variables. Of these, the most important is the distribution in the $\gamma\gamma$ center-of-mass energy $E_{\gamma\gamma}$, since this quantity determines the multiplicity of hadrons in the underlying event. In Figs. 9 and 10, we display the center-of-mass energy spectrum

$$E_{\gamma\gamma}\frac{dn}{dE_{\gamma\gamma}} \tag{4.3}$$

per bunch crossing for the canonical machine design described above, for $E_{c.m.} = 500$ GeV and 1 TeV e^+e^- and $\gamma\gamma$ colliders. These calculations assume the reference model. Note that the largest number of background events in e^+e^- colliders involve relatively low-energy $\gamma\gamma$ scattering processes. On the other hand, in a $\gamma\gamma$ collider, the luminosity spectrum of the background, like the spectrum of signal processes, peaks at the highest available energy.

For e^+e^- colliders, beamstrahlung is an important source of photons. Unfortunately, the results both for the number and spectrum of beamstrahlung photons depend on the details of the machine design and, in particular, on the number of particles per bunch and the bunch geometry. The disruption effect during the beam-beam collision further complicates the situation, as discussed in Sec. II. Thus, to assess the $\gamma\gamma$ backgrounds due to beamstrahlung, we must work with specific parameter sets for proposed colliders. In Table I, we list six proposed parameter sets for 500-GeV colliders [49]. For each of these, we have computed the number of $\gamma\gamma$ hadronic collisions per bunch crossing. In the table, we quote the values of $N_{\rm had}$, the total number of hadronic events, $N_{\rm jet5}$, the number of hadronic events with 5-GeV minijets (computed at $p_* = 3.2$ GeV), and $N_{\rm jet10}$, the number of events with 10-GeV minijets (computed at $p_* = 8$ GeV). Each of these numbers is integrated over the range $E_{\gamma\gamma} > 5$ GeV. We also quote the values of these parameters for the case in which the electron beams are converted to backscattered photon beams, assuming no loss of the nominal luminosity [50]. In Fig. 11, we show the distribution of $E_{\gamma\gamma}$ for two representative cases: the Japan Linear Collider (JLC) and TESLA. The corresponding spectra for the photon colliders can be obtained by scaling from Fig. 10(a), as we have remarked above.

We see from Table I that disruption effects have two major impacts on beamstrahlung and the $\gamma\gamma$ backgrounds. First, disruption hardens the beamstrahlung spectrum and increases its radiation rate. In addition, disruption enhances the luminosity per bunch crossing. In machine designs such as the CERN Linear Collider (CLIC), DESY-Darmstadt Linear Collider (DLC), and TESLA, for which the beams are not extremely flat, the horizontal disruption D_x can be quite large. This leads to an effective luminosity and concomitant beamstrahlung substantially different from the nominal designed values.

Care must be taken to include these effects when evaluating beamstrahlung and the backgrounds.

In estimating the size of the beamstrahlung-induced backgrounds, one should pay special attention to the parameter n_γ, the average number of beamstrahlung photons radiated per electron. Since in the collider energy range of our interest the hadron total cross section is reasonably constant in the $\gamma\gamma$ center-of-mass energy, the total hadronic event rate $N_{\rm had}$ scales roughly as the square of n_γ when $\bar{\mathcal{L}}_1$ is fixed. This is the source of the variation by almost two orders of magnitude among the first five machines of Table I in the total rate of hadronic events per bunch crossing. Since the minijet production comes dominantly from high-energy photons, the jet cross sections are less sensitive to n_γ. The sixth machine, the Serpukhov collider VLEPP, has a very different design philosophy from the first five in having only one bunch in a pulse train. This results in a luminosity per bunch crossing which is about 100 times larger than all other machines. When convoluted with a large number of beamstrahlung photons (mainly due to a large σ_z), VLEPP tends to produce the most hadronic event rates among all the machines.

Since there are no beamstrahlung and disruption effects involved in the $\gamma\gamma$ collision, the hadronic backgrounds in the $\gamma\gamma$ mode are very comparable among the first five machines listed in Table I.

In Table II, we present some representative designs for 1-TeV colliders and our estimate of the $\gamma\gamma$ background rates both in e^+e^- and $\gamma\gamma$ collider modes. For the e^+e^- collider designs, the $E_{\gamma\gamma}$ spectra for the cases of JLC and TESLA are shown in Fig. 12. Again, in the case of DLC and TESLA designs, the relatively larger disruption effects and n_γ lead to a much higher rate of hadronic events. Although the $\gamma\gamma$ reactions are mainly soft, one finds more than one jetlike underlying event per bunch crossing in these two cases. In the 1-TeV $\gamma\gamma$ collision mode, it is true for all four machines that typical events

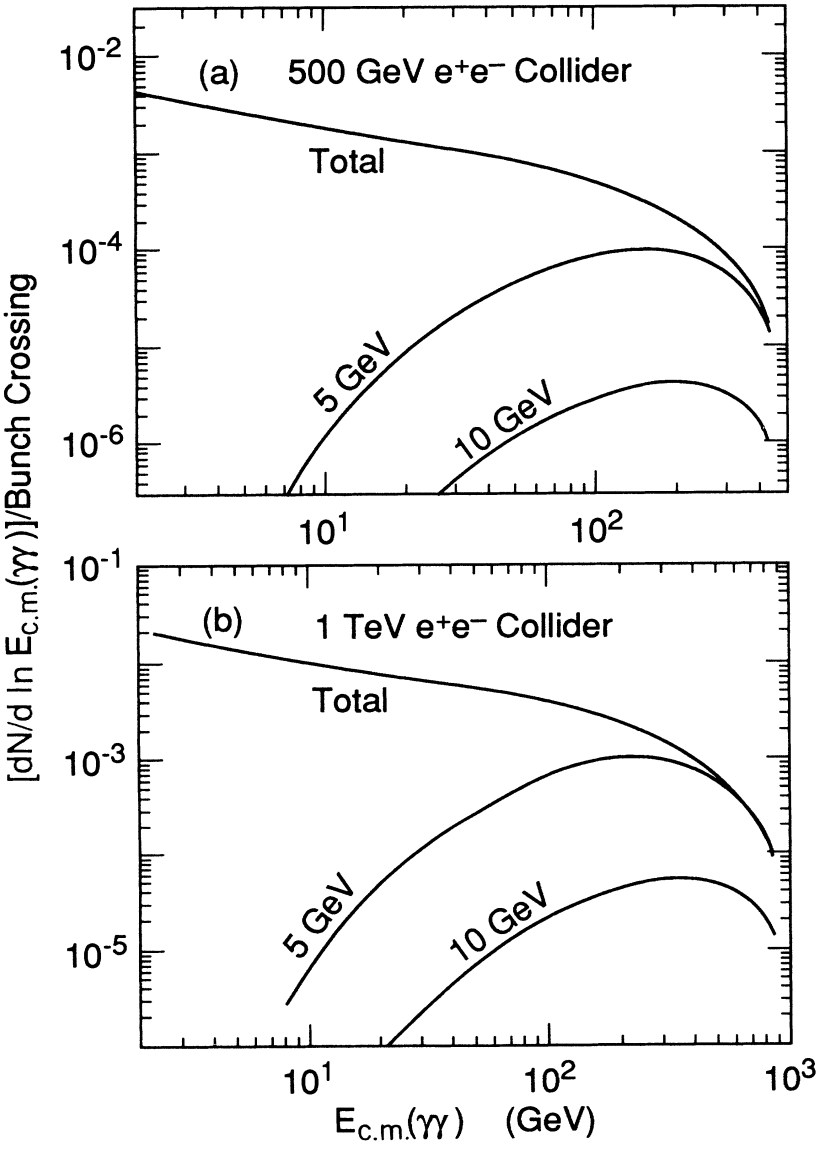

FIG. 9. Spectrum of $\gamma\gamma$ hadronic events in the $\gamma\gamma$ center-of-mass energy, $dn/d\ln E_{\gamma\gamma}$, produced in e^+e^- colliders at the canonical luminosity (4.2), from bremsstrahlung photons only. The three curves represent all $\gamma\gamma$ events, events with 5-GeV minijets, and events with 10-GeV minijet. The two cases are (a) 500-GeV collider and (b) 1-TeV collider.

have underlying hadronic events with QCD minijets. It is interesting to note that, with the differences from beamstrahlung removed in the $\gamma\gamma$ mode, the hadronic and minijet event rates for DLC and TESLA are comparable to those for JLC and NLC.

V. SIMULATION OF HADRONIC BACKGROUNDS

Now that we have computed the fraction of e^+e^- or $\gamma\gamma$ events at a linear collider which have underlying hadronic activity, we should still ask how these underlying hadronic events affect the analysis of high-energy event on which they may be superposed. There are good reasons to expect that the answer to this question should further diminish the importance of the Drees-Godbole background processes. The $\gamma\gamma$ collisions whose rates we computed in the previous section typically occur between photons of unequal energy, leading to a highly boosted final hadronic system. Even if this system contains minijets, it will include relatively few high-transverse-momentum particles. Thus most of the final hadrons will disappear down the beam pipe in the forward or backward direction. Unfortunately, we did not find a simple way to estimate the expectation for the resulting energy distributions, except by direct simulation. In this section, we will describe the results of a simulation of the background hadronic energy deposition based on our reference model.

According to Fig. 5, the qualitative form of hadronic background events will be different for the different sets of colliders we have considered. For the 500-GeV electron colliders, not only are there relatively few hadronic events per bunch crossing, but also those hadronic events are typically of minimum-bias type without minijets. On the other hand, the background events at a 1-TeV $\gamma\gamma$ collider typically contain several minijet pairs, depending on the transverse momentum criterion for a distinct minijet. We will present results for both of these cases.

To generate $\gamma\gamma$ hadronic events, we need an appropriate scheme for the simulation. Jets, when they occur,

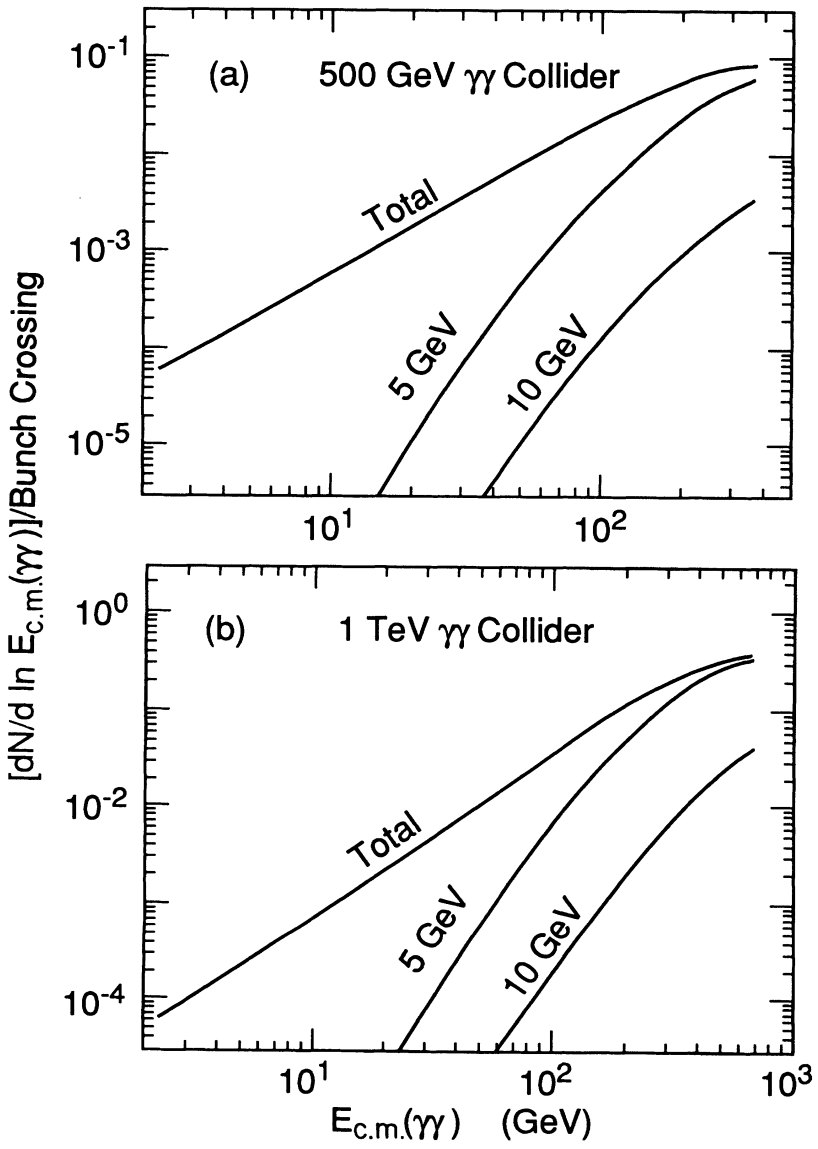

FIG. 10. Spectrum of $\gamma\gamma$ hadronic events in the $\gamma\gamma$ center-of-mass energy, $dn/d\ln E_{\gamma\gamma}$, produced in backscattered-laser $\gamma\gamma$ colliders at the canonical luminosity (4.2). The three curves are as in Fig. 9. The two cases are (a) 500-GeV collider and (b) 1-TeV collider.

could be modeled by parton fragmentation, but it is less clear how one should model the particle production from low-momentum-transfer processes. One method, which has been used by experimental groups investigating jet phenomena in $\gamma\gamma$ physics [51], is to model the soft part of the hadronic reaction as the fragmentation of an additional pair of partons. In this approach, it is straightforward to include the correct color coherence between the particle production by jets and by soft processes. However, this is not obviously the best way to treat soft processes without jets which make up the largest part of our event sample.

Instead, we have chosen to model the soft part of the reaction by applying the minimum-bias generator of the ISAJET Monte Carlo program [52]. Since this generator has been fit to data from minimum-bias events at the CERN Intersecting Storage Rings (ISR), SPS, and Fermilab Tevatron colliders, we have confidence that it will give a correct description of the soft hadronic physics up to the highest energies that we consider. The problem with this strategy is that it is very difficult to impose the cancellations in particle production which result from color coherence. In our simulation, we have chosen to add minijets incoherently to the soft background. Our expectation is that this strategy overestimates the particle production in the central region and thus gives a conservative estimate of the size of the hadronic background.

More specifically, we take the following model for $\gamma\gamma$ hadronic events. We first generate minijet pairs according to the reference model, using a Poisson distribution with mean given by (3.10). The energy and angle distributions of the minijets are computed according to (3.4), in particular, using the gluon and quark distributions in the photon given by Drees and Grassie [34]. This calculation requires a cutoff p_* on the transverse momentum transfer in the parton-parton collision; we have taken this cutoff to be either 3.2 or 8 GeV. As we explained in Sec. III, the first of these values would assign the production of clusters of 5 GeV transverse momentum to incoherent production of minijets, while the second value would make this assignment only for clusters of 10 GeV transverse momentum. The partons are fragmented into jets

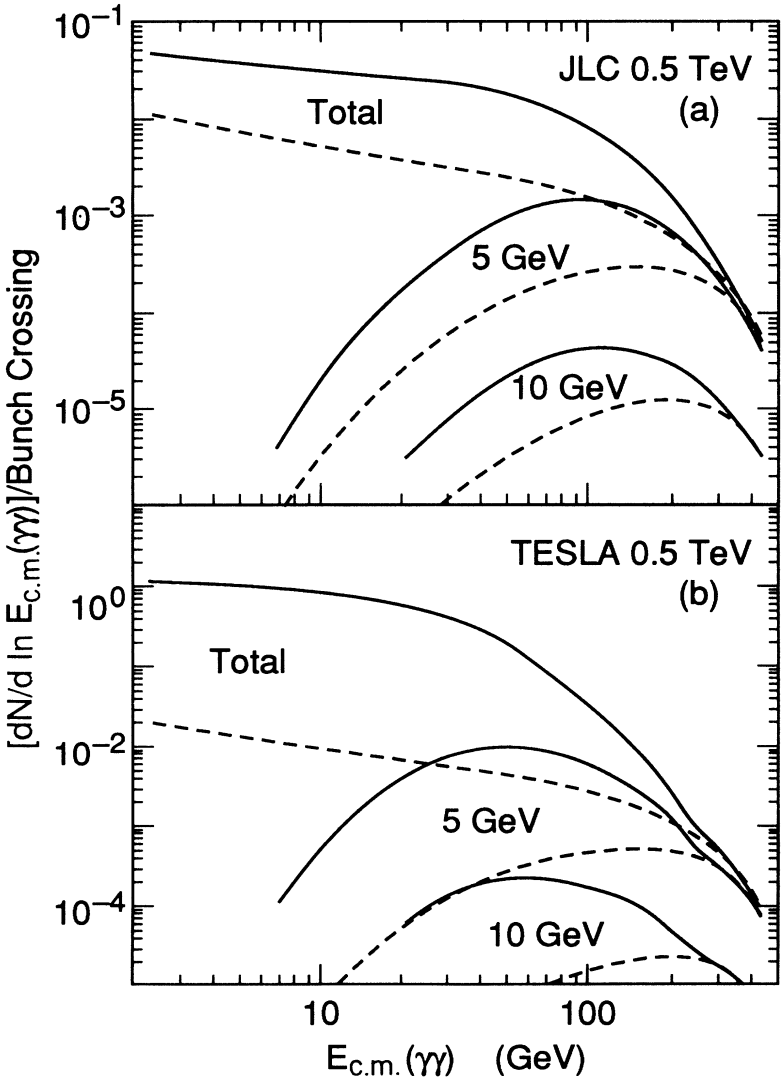

FIG. 11. Spectrum of $\gamma\gamma$ hadronic events, for two representative designs for 500-GeV e^+e^- colliders, following the parameters given in Table I. The three curves are as in Fig. 9. The dotted curves are the corresponding results for bremsstrahlung only. The two cases considered are (a) JLC and (b) TESLA.

using the LUND Monte Carlo program, version 6.3 [53]. Following the formation of all minijet pairs, the remaining energy is converted to hadrons using the minimum-bias event generator of the ISAJET Monte Carlo program. We modify this generator only in replacing the leading baryons by ρ^0's. We restrict our analysis to events with hadronic invariant mass at least 5 GeV.

To simulate the response of a detector to these events, we have used a model based on the features and resolution of the SLC large detector (SLD) [54]. As an important modification from the design of the SLD, we have assumed that the detector is blind to particles passing within 10° of the beam line ($|\cos\theta| > 0.985$). Planned detectors for future linear colliders include masking in this region to control the effects of electron-positron pairs produced in the collisions of electron and positron bunches, and simulations of physics signals at linear colliders incorporate this angular constraint.

From this model, we compute $E_{\rm dep}$, the total charged and neutral energy deposited in the detector by a single hadronic background event. We also compute a number of subsidiary quantities: To assess the effect of a stronger angular restriction, we have examined the quantity $E_{\rm dep}(0.9)$, the energy deposited in the angular region $|\cos\theta| < 0.9$. Most physics analyses for future linear colliders are insensitive to this restriction. Since missing transverse momentum signatures are important for some physics processes, we have computed $P_{\perp,\rm miss}$, the missing transverse momentum observed by the detector for the hadronic events. Finally, we have recomputed the observed missing transverse momentum using the stronger angular restriction, to define $P_{\perp,\rm miss}(0.9)$.

The results of this analysis are shown in Table III for three cases which represent the range of possibilities: first, the background hadronic events at a 500-GeV e^+e^- collider, second, the background hadronic events at a 1-TeV e^+e^- collider (in both cases, assuming the NLC design) and, finally, the hadronic events from monochromatic $\gamma\gamma$ collisions at 1 TeV in the center of mass. Note that the last case involves harder $\gamma\gamma$ collisions than

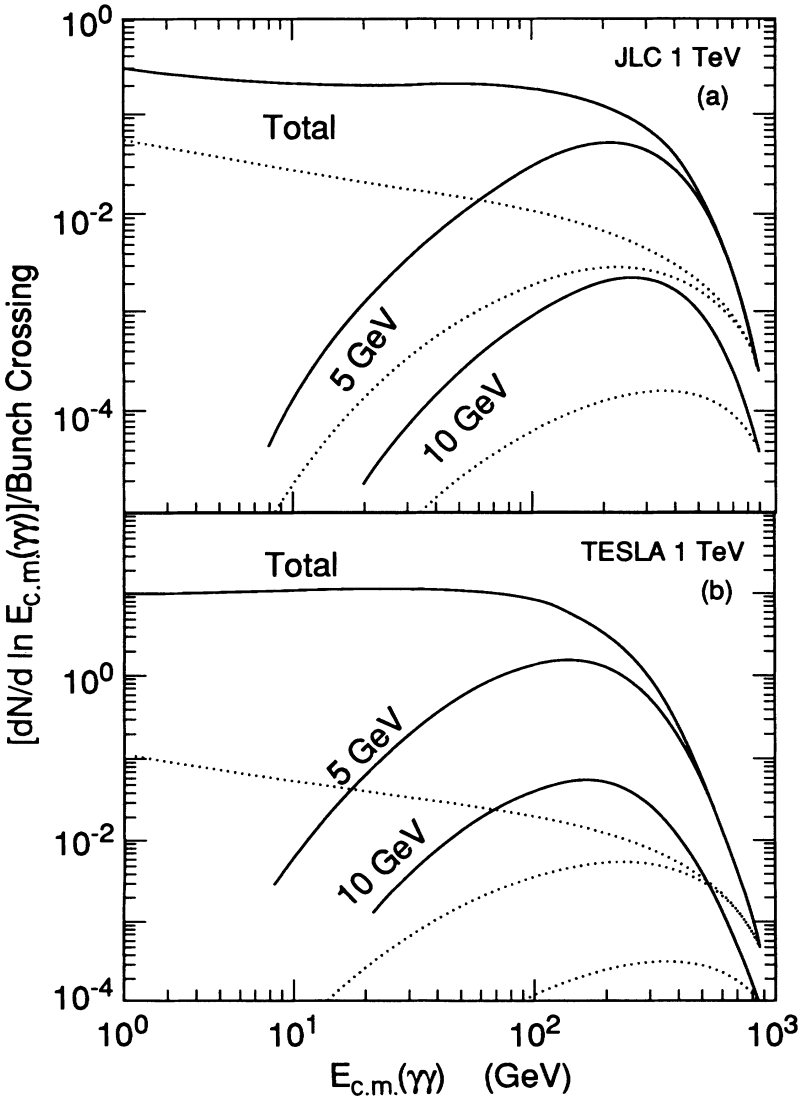

FIG. 12. Spectrum of $\gamma\gamma$ hadronic events, for two representative designs for 1-TeV e^+e^- colliders, following the parameters given in Table II. The three curves are as in Fig. 9. The dotted curves are the corresponding results for bremsstrahlung only. The figures correspond to (a) JLC and (b) TESLA.

TABLE III. Simulation results on hadronic backgrounds.

Linear colliders	NLC (500 GeV)	NLC (1 TeV)	$\gamma\gamma$ (1 TeV)	$\gamma\gamma$ (1 TeV)
p_*	3.2	3.2	3.2	8.0
$E_{\rm dep}$ (GeV)	8.0	11.0	64	33
st. dev.	7.1	11.6	31	25
$E_{\rm dep}(0.9)$ (GeV)	3.3	4.4	25	12
st. dev.	3.3	5.0	13	11
$P_{\perp,\rm miss}$ (GeV)	0.6	0.9	4.7	2.4
st. dev.	0.5	0.9	3.2	2.9
$P_{\perp,\rm miss}(0.9)$ (GeV)	0.7	0.9	5.0	2.3
st. dev.	0.6	1.0	3.6	3.1

one would find from the photon spectrum (2.17). In the first two cases, it is relatively rare that a hadronic event will contain a minijet pair, and so there is little difference between the results with $p_*=3.2$ and 8 GeV. In the third case, however, a typical hadronic event contains a 5-GeV minijet pair. Thus there is a considerable difference between the results for the two parameter choices, and this difference mainly reflects the explicit inclusion of the minijets in the former case. We have presented the results from both choices for comparison.

For the background events at e^+e^- colliders, we were surprised by the small values that the simulation produces, both for the energy deposition and for the missing transverse momentum. In Fig. 13, we display the distribution of $E_{\rm dep}$ and $E_{\rm dep}(0.9)$ computed for the 500-GeV NLC collider. The distributions fall off exponentially, with mean energy depositions of 7.9 and 3.3 GeV for $E_{\rm dep}$ and $E_{\rm dep}(0.9)$, respectively. The event numbers in the histogram of Fig. 13 correspond to an integrated luminosity of 0.5 pb^{-1}. This yields 40 000 hadronic background events, of which none has $E_{\rm dep}(0.9)$ greater than 50 GeV. If we include in the simulation hadronic events with invariant mass down to 1.6 GeV, this adds another 33 000 hadronic events, of which virtually all have $E_{\rm dep}$ less than 8 GeV and $E_{\rm dep}(0.9)$ less than 4 GeV. The missing transverse momentum in our sample of hadronic events is typically less than 1 GeV. Since the physics processes for which this is a signature typically have missing transverse momentum of order m_W, this small uncertainty is quite unimportant. The qualitative features of the hadronic background events, including the exponentially falling distribution in deposited energy, are the same for the 1-TeV e^+e^- collider.

For 1-TeV $\gamma\gamma$ collisions, the hadronic background events have a more serious effect and one which depends more strongly on the model used to generate these events.

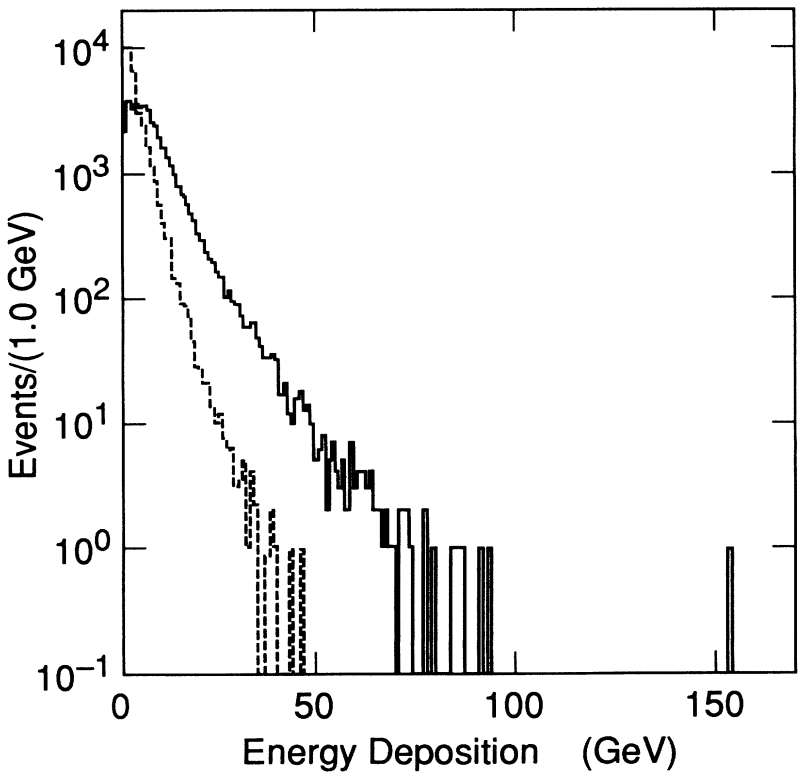

FIG. 13. Distribution of deposited energy for hadronic background events for a 500-GeV e^+e^- collider with a detector angular coverage of $|\cos\theta|<0.985$ (solid line) and of $|\cos\theta|<0.9$ (dashed line). The deposited energy is the sum of charged and neutral energy recorded by a detector, which is modeled as described in the text. The number of events corresponds to an integrated luminosity of 0.5 pb^{-1}.

In Fig. 14, we show the distribution in deposited energy for these events corresponding to 10 nb^{-1} of integrated luminosity. In Fig. 14(a), we generate hadronic events using $p_* = 3.2$ GeV. Then typical events contain at least one minijet pair. In Fig. 14(b), we assume $p_* = 8$ GeV, corresponding to the more restrictive hypothesis that minijets are not produced incoherently from the minimum-bias hadronic production mechanisms until they acquire a more substantial transverse momentum. We put forward both calculations to illustrate the possibilities. At a working $\gamma\gamma$ collider, it will of course be straightforward to measure this background and model it accurately. In either model, the background events deposit significant amounts of energy, but mostly in the extreme forward and backward directions. They add relatively little uncertainty to the determination of missing transverse momentum.

We argued in the previous section that, at e^+e^- linear colliders up to 1 TeV, only a small fraction of the e^+e^- annihilation events should have underlying background hadronic events generated by $\gamma\gamma$ collisions. Now it seems that, when such a background event does appear, it makes only a minor modification of the event pattern of the e^+e^- annihilation. For $\gamma\gamma$ colliders, especially at 1

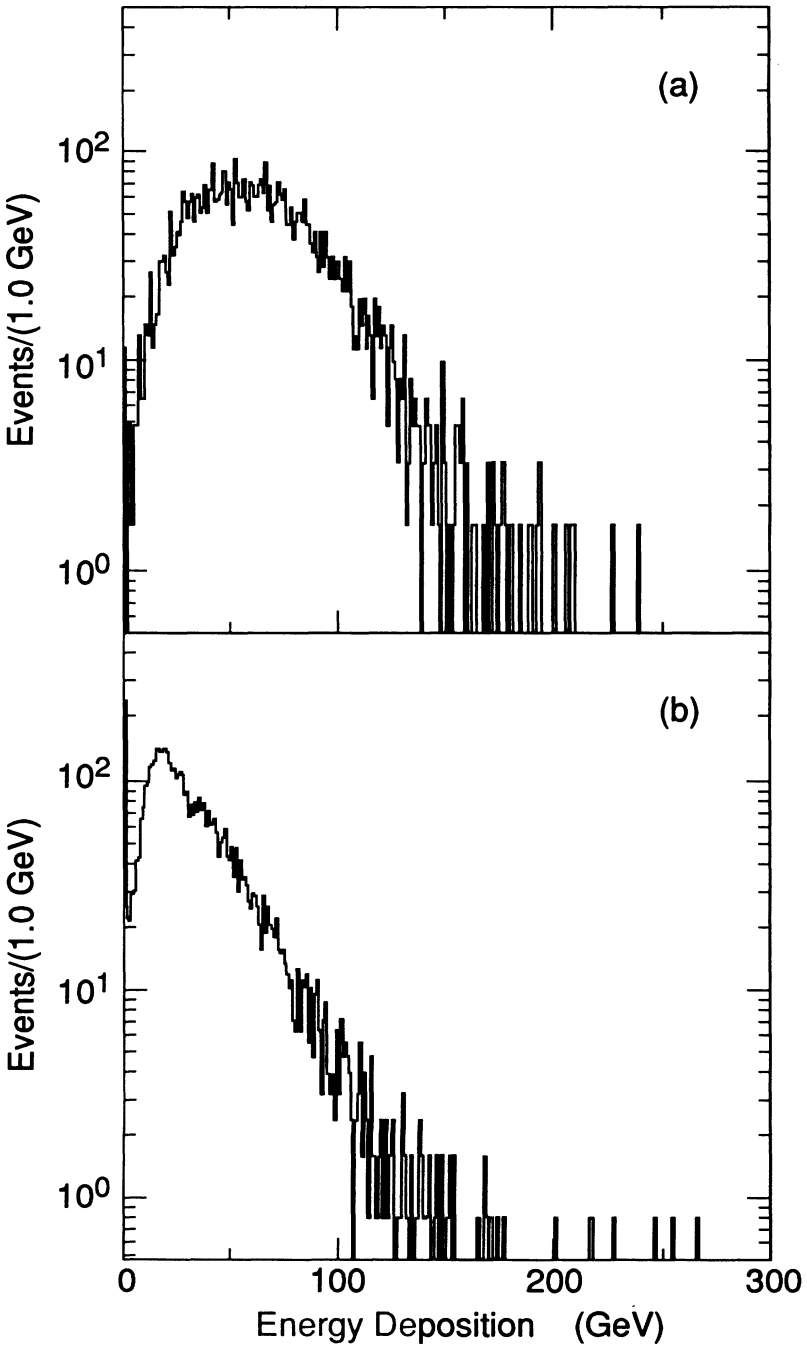

FIG. 14. Distribution of deposited energy for hadronic events in 1-TeV monochromatic $\gamma\gamma$ collisions, (a) computed with $p_* = 3.2$ GeV and (b) computed with $p_* = 8$ GeV. The number of events corresponds to an integrated luminosity of 10 nb^{-1}.

TeV, the background problem is more serious. Though the modification of the energy deposition in typical events is small, it is significant and should be taken into account in physics simulations.

VI. CONCLUSIONS

Drees and Godbole have called attention to the large rate of photon-photon collisions to be expected at future linear colliders and have suggested that the presence of underlying $\gamma\gamma$ events might be a serious source of background. To evaluate this claim, there are two issues that must be understood.

First, one must carefully evaluate the expected rate of soft and jetlike $\gamma\gamma$ events to be expected for given collider parameters. In this paper, we have presented what we feel is a useful solution to this problem. We have presented a physically correct picture of the hard and soft components of the $\gamma\gamma$ total cross section, and we have provided a set of formulas which allows this picture to be applied straightforwardly to compute the $\gamma\gamma$ rate for any collider design.

Second, one must ask whether such underlying hadronic events actually affect the experiments to be carried out at the next generation linear colliders. It is possible that any underlying event will compromise some aspects of linear collider physics. We have presented simulation results which indicate that the effect of this background will be minor at 500-GeV e^+e^- colliders, but that it will be more significant at higher energies, especially in the $\gamma\gamma$ collision mode. Even in 1-TeV $\gamma\gamma$ collisions, the Drees-Godbole background remains a relatively small perturbation of a high-energy reaction. In any event, we have given prescriptions which allow the Drees-Godbole background to be correctly included in simulations of physics processes to assess its effects directly.

As a final note, we should point out that there are strategies for reducing the Drees-Godbole backgrounds in e^+e^- colliders by readjusting the beam parameters. For example, by increasing the collision rate while lowering the bunch population and by colliding extremely flat beams, one may decrease the $\gamma\gamma$ reaction rates while retaining the total luminosity. We hope that the case studies and approximation schemes presented in this paper will be useful in further optimizing the designs for linear colliders.

ACKNOWLEDGMENTS

We are deeply grateful to James Bjorken for helping us to understand the basic physical picture which is used in this paper. We also thank Karl Berkelman, Manuel Drees, Rohini Godbole, John Storrow, and Valery Telnov for enlightening discussions. This work was supported by the Department of Energy, contract No. DE-AC03-76SF00515.

[1] P. Chen and R. J. Noble, Report No. SLAC-PUB-4050 1986 (unpublished); M. Bell and J. S. Bell, Part. Accel. **24**, 1 (1988); R. Blankenbecler and S. D. Drell, Phys. Rev. Lett. **61**, 2324 (1988); P. Chen and K. Yokoya, *ibid.* **61**, 1101 (1988); M. Jacob and T. T. Wu, Nucl. Phys. **B303**, 389 (1988); V. N. Baier, V. M. Katkov, and V. M. Strakhovenko, *ibid.* **B328**, 387 (1989).

[2] P. Chen and V. L. Telnov, Phys. Rev. Lett. **63**, 1796 (1989); R. Blankenbecler, S. D. Drell, and N. Kroll, Phys. Rev. D **40**, 2462 (1989); M. Jacob and T. T. Wu, Nucl. Phys. **B327**, 285 (1989).

[3] M. Drees and R. M. Godbole, Phys. Rev. Lett. **67**, 1189 (1991).

[4] M. Drees and R. M. Godbole, Report No. DESY 92-044, BU 92/1, 1992 (unpublished).

[5] I. F. Ginzburg, G. L. Kotkin, V. G. Serbo, and V. I. Telnov, Nucl. Instrum. Methods **205**, 47 (1983); I. F. Ginzburg, G. L. Kotkin, S. L. Panfil, V. G. Serbo, and V. I. Telnov, *ibid.* **219**, 5 (1984).

[6] T. Barklow, in *Research Directions for the Decade,* Proceedings of the Summer Study, Snowmass, Colorado, 1990, edited by E. L. Berger (World Scientific, Singapore, 1991).

[7] V. I. Telnov, in *Physics and Experiments with Linear Collider,* Saariselkä, Finland, 1991, edited by P. Orava, P. Eerola, and M. Nordberg (World Scientific, Singapore, 1992).

[8] D. L. Borden, D. A. Bauer, and D. O. Caldwell, Report No. SLAC-PUB-5715, UCSB-HEP-92-01, 1992 (unpublished).

[9] ZEUS Collaboration, M. Derrick *et al.*, Phys. Lett. B **293**, 465 (1992).

[10] H1 Collaboration, T. Ahmed *et al.*, Phys. Lett. B **299**, 374 (1993).

[11] J. R. Forshaw and J. K. Storrow, Phys. Lett. B **278**, 193 (1992).

[12] K. Berkelman, CLIC Note 164, May 1992; CLIC Note 168, July 1992.

[13] A. Miyamoto, in *Proceeding of the Third Workshop on Japan Linear Collider (JLC),* edited by A. Miyamoto (KEK, Tsukuba, 1992).

[14] T. Tauchi and H. Hayashi, in *Proceedings of the Workshop on Physics and Experiments with Linear Colliders,* edited by X. Tata (World Scientific, Singapore, in press, 1993).

[15] I. F. Ginzburg, D. Yu. Ivanov, and V. G. Serbo, in *Proceedings of the Workshop on Physics and Experiments with Linear Colliders* [13].

[16] A. E. Blinov *et al.*, Phys. Lett. **113B**, 423 (1982); Yu. A. Tikhonov, candidates dissertation, Institute Nuclear Physics, Novosibirsk, 1982; V. N. Baier, V. M. Katkov, and V. M. Strakhovenko, Yad. Fiz. **36**, 163 (1982) [Sov. J. Nucl. Phys. **36**, 95 (1982)]; A. I. Burov and Ya. S. Derbenev, INP Report No. 82-07, Novosibirsk, 1982 (unpublished); G. L. Kotkin, S. I. Polityko, and V. G. Serbo, Yad. Fiz. **42**, 692 (1985) [Sov. J. Nucl. Phys. **42**, 440 (1985)]; P. Chen, T. Tauchi, and D. V. Schroeder, in *Research Directions for the Decade* [6].

[17] S. Brodsky, T. Kinoshita, and H. Terazawa, Phys. Rev. D **4**, 1532 (1971).

[18] For the case of electron-hadron scattering, a more detailed computation of this suppression factor has been made by F. M. Borzumati and G. A. Schuler, Z. Phys. C **58**, 139 (1993).

[19] R. J. Noble, Nucl. Instrum. Method A **256**, 427 (1987).

[20] P. Chen, in *Frontiers of Particle Beams,* Lecture Notes in Physics Vol. 296 (Springer-Verlag, Berlin, 1988).

[21] R. Hollebeek, Nucl. Instrum. Methods **184**, 333 (1981).
[22] P. Chen and K. Yokoya, Phys. Rev. D **38**, 987 (1988); K. Yokoya and P. Chen, in *Frontiers of Particle Beams: Intenstiy Limitations,* Lecture Notes in Physics Vol. 400 (Springer-Verlag, Berlin, 1992).
[23] K. Yokoya, KEK Report No. 85-9, 1985 (unpublished).
[24] P. Chen, in *Photon-Photon Collisions,* Proceedings of the IXth International Workshop on Photon-Photon Collisions, edited by D. O. Caldwell and H. P. Paar (World Scientific, Singapore, 1992).
[25] J. B. Rosenzweig and P. Chen, in *Proceedings of IEEE Particle Accelerator Conference 91CH3038-7,* edited by M. Allen (IEEE Service Center, New York, 1991).
[26] P. Chen, Phys. Rev. D **46**, 1186 (1992).
[27] V. I. Telnov, Nucl. Instrum. Methods A **294**, 72 (1990).
[28] U. Amaldi *et al.*, Phys, Lett. **66B**, 390 (1977).
[29] PLUTO collaboration, Ch. Berger *et al.*, Phys. Lett. **149B**, 421 (1984).
[30] TPC/Two-Gamma collaboration, H. Aihara *et al.*, Phys. Rev. D **41**, 2667 (1990).
[31] MD-1 collaboration, S. E. Baru *et al.*, Novosibirsk Report No. IYF-91-52, 1991 (unpublished).
[32] M. Drees and F. Halzen, Phys. Rev. Lett. **61**, 275 (1988).
[33] B. L. Combridge and C. J. Maxwell, Nucl. Phys. **B239**, 429 (1984).
[34] M. Drees and K. Grassie, Z. Phys. C **28**, 451 (1985).
[35] L. E. Gordon and J. K. Storrow, Z. Phys. C **56**, 307 (1992).
[36] H. Abramowicz, M. Krawczyk, K. Charchula, A. Levy, and U. Maor, Int. J. Mod. Phys. A **8**, 1005 (1993).
[37] E. A. Kuraev, J. N. Lipatov, and V. S. Fadin, Zh. Eksp. Teor. Fiz. **72**, 377 (1977) [Sov. Phys. JETP **45**, 199 (1977)]; Ya. Ya. Balitsky and L. N. Lipatov, Yad. Fiz. **28**, 1597 (1978) [Sov. J. Nucl. Phys. **28**, 822 (1978)].
[38] A second possible source of suppression, the saturation of the gluon evolution at small z, has been discussed by Collins and Ladinsky [40]. However, this effect is small in the energy region we consider in this paper.
[39] L. Durand and H. Pi, Phys. Rev. Lett. **58**, 303 (1987), Phys. Rev. D **40**, 1436 (1989).
[40] J. Collins and G. Ladinsky, Phys. Rev. D **43**, 2847 (1991).
[41] S. I. Alekhin *et al.*, Report No. CERN-HERA 87-01, 1987 (unpublished).
[42] UA1 experiment, C. Albajar *et al.*, Nucl. Phys. **B309**, 405 (1988).
[43] G. Pancheri and Y. Srivastava, Phys. Lett. B **182**, 199 (1986).
[44] J. R. Forshaw and J. K. Storrow, Phys. Lett. B **268**, 116 (1991); **276**, 565E (1992).
[45] R. S. Fletcher, T. K. Gaisser, and F. Halzen, Phys. Rev. D **45**, 377 (1992).
[46] M. M. Block, R. Fletcher, F. Halzen, B. Margolis, and P. Valin, Phys. Rev. D **41**, 978 (1990).
[47] "LC92 Proceedings," edited by R. Settles, ECFA Report No. 92/46, 1992 (unpublished).
[48] The 1.0-TeV designs are taken from the following sources: DLC: G. Voss and T. Weiland, SLAC Beam Line **22** (1), 24 (1992); JLC: K. Yokoya (private communication); NLC: R. Ruth (private communication); TESLA: H. Padamsee, "TESLA Calculations Program," Cornell report, 1991 (unpublished).
[49] For the case of VLEPP, the prescription of Sec. II fails due to the large value of σ_z/β_y^*. The correct remedy [V. Balakin (private communication)] is to set $H_{D_y}=1$ and proceed from Eq. (2.9).
[50] For e^+e^- colliders, we estimate event rates using the enhanced luminosity per bunch $\overline{\mathcal{L}}_1$. For $\gamma\gamma$ colliders, we use the unenhanced luminosity $\mathcal{L}_1$.
[51] AMY Collaboration, R. Tanaka *et al.*, Phys. Lett B **277**, 215 (1992).
[52] F. E. Paige and S. D. Protopopescu, in *Physics of the Superconducting Supercollider, Snowmass, 1986,* Proceedings of the Summer Study, Snowmass, Colorado, edited by R. Donaldson and J. Marx (Divisoin of Particles and Fields of the APS, New York, 1987).
[53] T. Sjöstrand, Comput. Phys. Commun. **39**, 347 (1986); M. Bengtsson and T. Sjöstrand, Nucl. Phys. **B289**, 810 (1987).
[54] "The SLD Design Report," SLAC Report No. 273, 1984 (unpublished).